28

Excitation of nucleon resonances

One of the primary goals of electron scattering experiments is to understand the internal structure of the nucleon, both its static and dynamic properties. Ultimately, electron scattering data will provide benchmarks against which the theoretical predictions of QCD can be compared.

Elastic scattering from the nucleon has been discussed in chapter 22. There are no discrete bound states of the nucleon as there are in nuclei, and thus excited states of the nucleon show up as resonances in particle production processes. This is analogous to the situation with giant resonances in nuclei which lie above particle emission threshold. Nucleon resonances are characterized by strong interaction widths, a typical value for which is given by the time it takes a light signal to travel a pion Compton wavelength, or $\Gamma \approx \hbar c/(\hbar/m_\pi c) \approx m_\pi c^2 \approx 135\,\mathrm{MeV}$.

The first inelastic process on the nucleon occurs with the production of the lightest hadron, the pion. The coincidence cross section for the reaction $\mathrm{N(e,e'\pi)N}$ follows immediately from the general analysis in chapter 13. The angular distribution in the C-M system for arbitrary nucleon helicities is given by Eq. (13.68). If the nucleon target is unpolarized and its final polarization unobserved, the angular distribution reduces to that given in Eqs. (13.71) and (F.9). The analysis of pion electroproduction starting from the covariant, gauge invariant S-matrix and reducing it to the contribution of multipoles leading to states of definite J^π in the final π–N system is presented in detail in appendix H. Such a decomposition forms the basis for current phenomenological analyses of coincident electron scattering experiments aimed at extracting properties of nucleon resonances. Existing pion electroproduction data is presented in [Br82, Br83, Fo83] and discussed further in [Bu94]. The reader is referred to these references for previous applications.

To get some idea of the quality of the data that is now becoming

https://doi.org/10.1017/9781009290616.033 Published online by Cambridge University Press

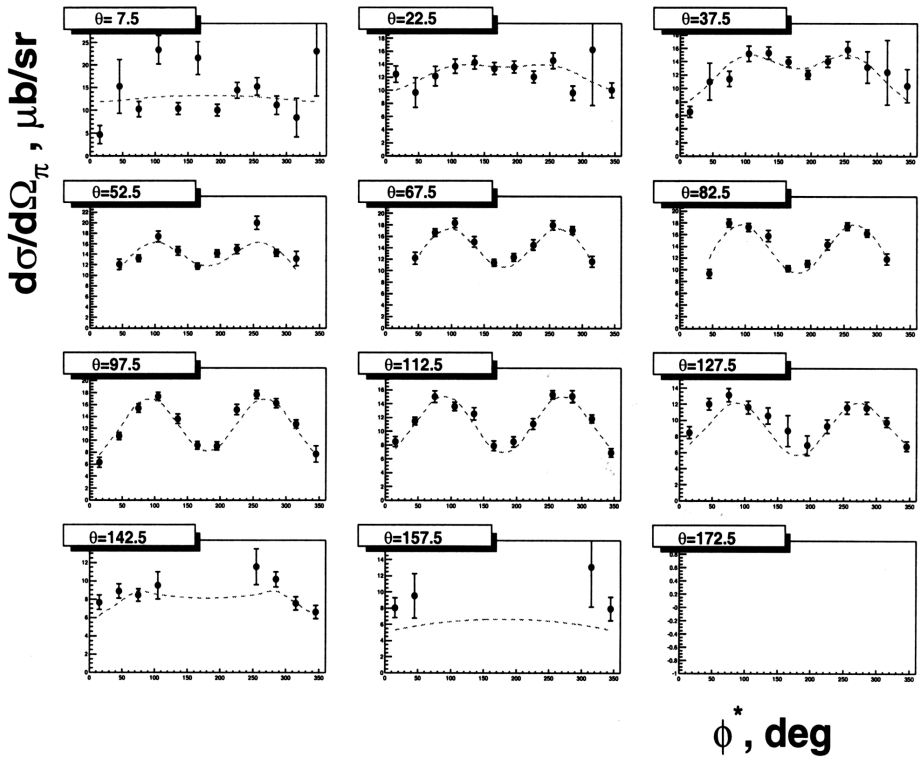

Fig. 28.1. Preliminary angular distribution data $d\sigma/d\Omega_q$ in μb/sr for process p(e, e′ π^+)n on the first nucleon resonance from Hall B collaboration at TJNAF [Eg01]. Here $k^2 = 0.40\,(\mathrm{GeV}/c)^2, W = 1.230\,\mathrm{GeV}/c^2, \Delta k^2 = 0.100\,(\mathrm{GeV}/c)^2$, and $\Delta W = 0.020\,\mathrm{GeV}/c^2$. The plots are vs. $\phi^\star = \pi/2 - \phi_q$ for various θ_q. The author is grateful to H. Egiyan for preparing this figure.

available on the coincident electropion production process, we show in Fig. 28.1 some of the very first results for the process p(e, e′ π^+)n from the Hall B collaboration at TJNAF [Eg01].

QCD-inspired models of the internal structure of the nucleon give rise to a rich structure of dynamic excitations. One now has a quark-based picture of the underlying structure similar to that of the periodic table of the elements in atomic physics, or the shell model in nuclear physics [Bh88, Wa95]. The M.I.T. bag models confinement and asymptotic freedom with three massless quarks moving in a vacuum bubble [Ch74, Ch74a, De75, Ja76]. The constituent quark model has three non-relativistic quarks with masses $m_q \approx M/3$ moving in a confining potential, for example, a harmonic oscillator [Is77, Is80, Is81, Is85]. Electron scattering coincidence studies of reactions proceeding through these resonances N(e, e′)N* →

https://doi.org/10.1017/9781009290616.033 Published online by Cambridge University Press

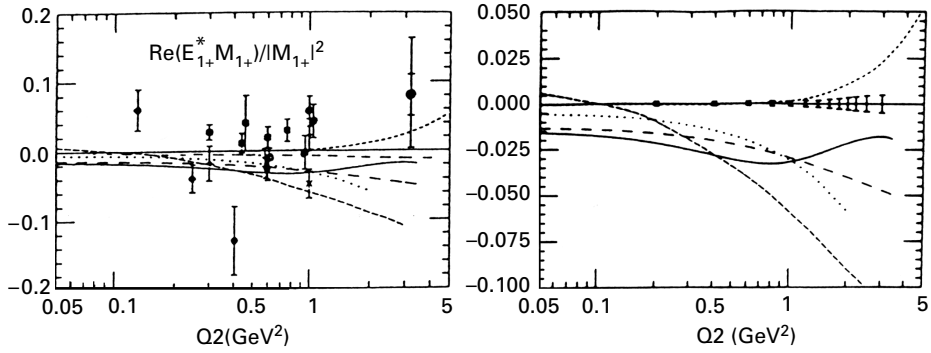

Fig. 28.2. (left) Existing world's data on $\mathrm{Re}\,(E^*_{1+}M_{1+})/|M_{1+}|^2$ at the $\Delta(1232)$ as of CEBAF PR89-037 [Bu89, Wa93]. Here $k \equiv Q$.

Fig. 28.3. (right) Projected range and error bars on $\mathrm{Re}\,(E^*_{1+}M_{1+})/|M_{1+}|^2$ at the $\Delta(1232)$ in CEBAF PR89-037 [Bu89, Wa93]. Here $k \equiv Q$.

N(e, e′ X)N promise to teach us much about the internal dynamics of the nucleon [Bu94].[1]

The quark model prediction for electron excitation of the first excited state of the nucleon, the $\Delta(1232)$, has been examined in chapter 24. It is clear from Fig. 12.8 that this first excited state is seen experimentally as a nice, isolated resonance.

The electric quadrupole transition amplitude E_{1+} to the $\Delta(1232)$ with $(J^\pi, T) = (\frac{3}{2}^+, \frac{3}{2})$ is particularly interesting. Quark bag models of the nucleon, with a one-gluon exchange interaction, indicate that the bag may deform — similar to the deformation of the deuteron arising from the tensor force. As with even–even deformed nuclei, the nucleon can have no quadrupole moment in its ground state, so the most direct evidence for such an intrinsic deformation would show up in this transition amplitude. In the quark model, the transition amplitude to the $P_{33}(1232)$ is predominantly a spin-flip magnetic dipole M_{1+}. The E_{1+} is, in fact, observed to be small, and it is currently only very poorly known. This is illustrated in Fig. 28.2, which shows the existing world's data on $\mathrm{Re}\,(E^*_{1+}M_{1+})/|M_{1+}|^2$ at the $\Delta(1232)$ as of the proposal CEBAF PR 89-037 [Bu89]. Figure 28.3 shows the projected range and error bars in that proposal [Bu89]. Note, in particular, the expansion of the vertical scale in this second figure. At TJNAF (CEBAF), the internal dynamics of the nucleon will be studied with unrivaled precision. These measurements will provide *deep insight into the dynamical consequences of QCD*. The accurate new data will continue to

[1] See this review article [Bu94] for an extensive list of further references on electron excitation of the nucleon and the quark model.

https://doi.org/10.1017/9781009290616.033 Published online by Cambridge University Press

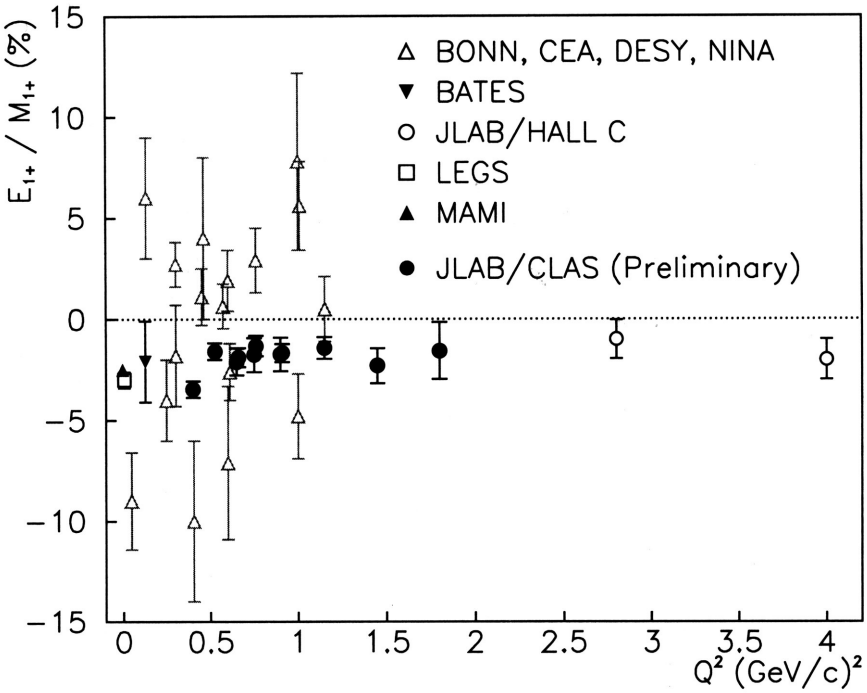

Fig. 28.4. Preliminary results obtained for E_{1+} by the Hall B collaboration at TJNAF from the reaction p(e, e′π^0)p [HB01]. The author is grateful to V. Burkert and C. Smith for the preparation of this figure.

provide *benchmark tests for theoretical quark-model and QCD descriptions of the nucleon — the basic building block of matter.*

Figure 28.4 shows actual data on this ratio obtained from an analysis of the process p(e, e′ π^0)p by the Hall B collaboration at TJNAF [HB01]. Note the quality of these results.

It is evident from Fig. 12.8 and the Particle Data Book that the higher nucleon resonances are many, broad, and overlapping. It will be a challenge to isolate the individual resonance contributions, particularly when there is a substantial background contribution as is evident from Fig. 12.8. A second challenge is to have a completely relativistic description of the quark bound-state structure of the nucleon; this is essential when one goes to momentum transfers $k^2 \gg m_q^2$.[2]

As first shown in a non-relativistic static model by Chew and Low [Ch56a], and subsequently generalized to the relativistic case [Ch57, Fr60], the Δ(1232) can be alternatively obtained as a dynamic resonance in a pion–nucleon field theory (QHD). Here, instead of starting at short

[2] Relativistic corrections to the constituent quark model are examined in [Ca86, Ca87].

https://doi.org/10.1017/9781009290616.033 Published online by Cambridge University Press

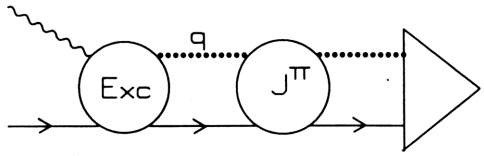

Fig. 28.5. Electroexcitation of the first nucleon resonance.

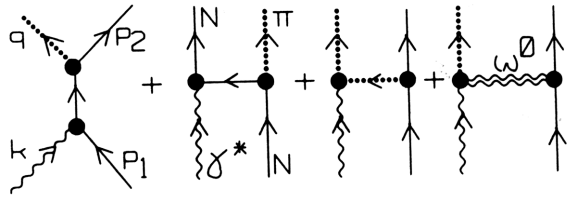

Fig. 28.6. Generalized Feynman amplitude used as the excitation mechanism in the $|\pi N\rangle$ channel for the $\Delta(1232)$ [Pr69, Wa72]. It is assumed that $F_\pi \approx F_1^V$. [For the last graph, which plays a minor role for the $\Delta(1232)$, $g_{\omega\pi\gamma}$ is obtained from $\omega \to \pi + \gamma$, and $g_{\omega\pi\gamma} g_{\omega NN}$ from an overall fit to the inelastic resonance spectra; it is assumed that $F_{\omega\pi\gamma} \approx F_2^V / F_2^V(0)$.]

distances with an asymptotically free quark model, one starts at large distances with a pion–nucleon description of the structure of the nucleon. Electron excitation of this resonance can then be viewed as an excitation process into the proper π–N channel followed by a dynamic final-state enhancement that builds up the resonance, as illustrated in Fig. 28.5.

As a model for $\mathrm{N(e,e')}\Delta$ consider the following [Wa68, Pr69, Wa72]

$$\begin{aligned} a(W,k^2) &= \frac{a^{\mathrm{lhs}}(W,k^2)}{D(W)} \\ D(W) &= \exp\left\{-\frac{1}{\pi}\int_{W_0}^{\infty} \frac{\delta(W')\,dW'}{W' - W - i\varepsilon}\right\} \end{aligned} \tag{28.1}$$

Here $a^{\mathrm{lhs}}(W,k^2)$ is the appropriate multipole projection of a set of Feynman graphs thought to play an important role in the excitation of the resonance and $D(W)$ is a final-state enhancement factor. The sum of excitation graphs is treated as a generalized Feynman amplitude in that renormalized coupling constants and electromagnetic form factors $F(k^2)$ are used at the vertices; the justification for this procedure is that this amplitude has the correct left-hand singularity structure arising from the pole terms in a dispersion treatment of this process [Fu58]. The graphs used in the present calculation [Wa68, Pr69, Wa72] are shown in Fig. 28.6. The multipole projections are obtained through the analysis in appendix H.

https://doi.org/10.1017/9781009290616.033 Published online by Cambridge University Press

The excitation amplitude arising from the first three graphs is constructed below.

Division of numerator and denominator in Eq. (28.1) by $D(M_s)$ changes nothing and

$$\frac{D(W)}{D(M_s)} = \exp\left\{-\frac{(W-M_s)}{\pi}\int_{W_0}^{\infty}\frac{\delta(W')\,dW'}{(W'-M_s)(W'-W-i\varepsilon)}\right\} \quad (28.2)$$

This relation provides additional convergence. If one assumes that $a(W,k^2) \equiv a^{\text{lhs}}(W,k^2)$ at a given point, as in [Ch56a] where in the static limit one has a simple pole at $W = M$, then the quantity M_s is determined.[3]

This is a very simple model; but, it has several features to recommend it:

1. It has the correct analytic properties since $a^{\text{lhs}}(W,k^2)$ has the correct left-hand singularities and $D(W)$ has the right-hand unitarity cut;
2. It has the correct threshold behavior in both $|\mathbf{k}^*|$ and $|\mathbf{q}|$ [Bj66];
3. It satisfies Watson's theorem $a = |a|e^{i\delta}$ on the physical cut [Wa52]; here δ is the strong interaction π–N phase shift (see appendix H);
4. It is an approximate solution to the integral equation of Omnès [Om59];
5. The electroproduction amplitude resonates at the same W_R as elastic scattering;
6. The calculation is completely relativistic;
7. The current is conserved;
8. The k^2 dependence is explicit.

Let us elaborate on some of these points. The problem of constructing an analytic function $a(W,k^2)$ with a specified set of left-hand singularities in W given by $a^{\text{lhs}}(W,k^2)$, where $a^{\text{lhs}}(W,k^2)$ is real on the physical real axis and where the overall amplitude obeys Watson's theorem there, was formulated by Omnès as an integral equation [Om59]

$$a(W,k^2) = a^{\text{lhs}}(W,k^2) + \frac{1}{\pi}\int_{W_0}^{\infty}\frac{e^{-i\delta(W')}\sin\delta(W')\,a(W',k^2)}{W'-W-i\varepsilon}dW' \quad (28.3)$$

[3] The calculation shown uses $M_s = 0.95M$ and $\text{Re}\,\delta(W)$ everywhere in the integral.

https://doi.org/10.1017/9781009290616.033 Published online by Cambridge University Press

The solution to this integral equation for $W_0 \leq W \leq \infty$ was also given by Omnès [Om59]

$$\begin{aligned} a(W,k^2) &= e^{i\delta(W)}\left[a^{\text{lhs}}(W,k^2)\cos\delta(W)\right. \\ &\left. +e^{\rho(W)}\frac{\mathscr{P}}{\pi}\int_{W_0}^{\infty}\frac{a^{\text{lhs}}(\xi,k^2)\sin\delta(\xi)e^{-\rho(\xi)}}{\xi-W}d\xi\right] \end{aligned} \tag{28.4}$$

In this expression $\mathscr{P}$ is the Cauchy principal value and

$$\rho(W) = \frac{\mathscr{P}}{\pi}\int_{W_0}^{\infty}\frac{\delta(\zeta)\,d\zeta}{\zeta-W} \tag{28.5}$$

Assume now that $a^{\text{lhs}}(W,k^2)$ varies only slowly over the region where $\sin\delta(W) \neq 0$ on the physical cut, and factor it out of the integral. It then follows that

$$\begin{aligned} a(W,k^2) &\approx a^{\text{lhs}}(W,k^2)\,\chi(W) \\ \chi(W) &= \psi(W)\,\exp\left\{\frac{1}{\pi}\int_{W_0}^{\infty}\delta(W')\,dW'\frac{1}{W'-W-i\varepsilon}\right\} \\ \psi(W) &= \exp\left[-\frac{1}{\pi}\int_{W_0}^{\infty}\frac{\delta(W')\,dW'}{W'-W-i\varepsilon}\right] \\ &\quad +\frac{1}{\pi}\int_{W_0}^{\infty}\frac{\sin\delta(\xi)\,d\xi}{\xi-W-i\varepsilon}\exp\left[-\frac{\mathscr{P}}{\pi}\int_{W_0}^{\infty}\frac{\delta(\zeta)\,d\zeta}{\zeta-\xi}\right] \end{aligned} \tag{28.6}$$

The evident analytic properties of $\psi(W)$, and the observation that $\psi \to 1$ as $|W| \to \infty$, allow one to write an unsubtracted dispersion relation for $\psi(W) - 1$. A simple calculation shows that on the right-hand physical cut the discontinuity of this function vanishes, hence one concludes that $\psi(W) \equiv 1$!

It follows that

$$\begin{aligned} a(W,k^2) &= \frac{a^{\text{lhs}}(W,k^2)}{D(W)} \\ D(W) &= \exp\left[-\frac{1}{\pi}\int_{W_0}^{\infty}\frac{\delta(W')\,dW'}{W'-W-i\varepsilon}\right] \end{aligned} \tag{28.7}$$

This is just Eq. 28.1. Here $D(W)$ serves as a final-state enhancement factor, and this final-state enhancement factor satisfies Watson's theorem

$$D(W) = |D(W)|e^{-i\delta(W)} \qquad ;\ W \geq W_0 \tag{28.8}$$

$D(W)$ is purely imaginary at a resonance in elastic scattering where $\delta(W_R) = \pi/2$. A Taylor series around the resonance then gives

$$D(W) \approx (W - W_R)\left[\frac{d\,\text{Re}\,D(W)}{dW}\right]_{W=W_R} + i\,\text{Im}\,D(W_R) \tag{28.9}$$

https://doi.org/10.1017/9781009290616.033 Published online by Cambridge University Press

The electroproduction amplitude in this channel then resonates at the same W_R and has a Breit–Wigner form.

Finally, consider the Feynman diagrams in Fig. 28.6 as the excitation mechanism for the production of the low-lying nucleon resonances in Fig. 12.8. Treat these as generalized Feynman amplitudes using renormalized coupling constants and physical electromagnetic form factors $F(k^2)$ at the vertices; again, the justification for this procedure is that these terms give the correct pole contributions in the dispersion relations for the electroproduction amplitudes [Fu58]. The contribution of the nucleon and pion pole terms takes the form [Wa95]

$$\left(\frac{4\pi W}{M}\right)\mathscr{J}_\lambda^{\text{pole}}\varepsilon_\lambda = -g_\pi \bar{u}(p_2)\left\{\tau_\alpha M_\lambda^{(0)} + \delta_{\alpha 3} M_\lambda^{(+)} + \frac{1}{2}[\tau_\alpha, \tau_3] M_\lambda^{(-)}\right\} u(p_1)\varepsilon_\lambda$$

$$\begin{aligned} M_\lambda^{(i)} &= \gamma_5 \frac{1}{i(\not{p}_1 + \not{k}) + M}[F_1^{(i)}\gamma_\lambda - F_2^{(i)}\sigma_{\lambda\rho}k_\rho] \\ &\quad + s_i[F_1^{(i)}\gamma_\lambda - F_2^{(i)}\sigma_{\lambda\rho}k_\rho]\frac{1}{i(\not{p}_2 - \not{k}) + M}\gamma_5 \\ &\quad - if_i\gamma_5 \frac{(2q-k)_\lambda}{(q-k)^2 + \mu^2} F_\pi \end{aligned} \tag{28.10}$$

Here the spinor normalization is $\bar{u}u = 1$, the Feynman notation $\not{a} = a_\mu\gamma_\mu$ is employed, and the form factors are given by

$$\begin{aligned} 2F^{(0)} &= F^S \quad ; s_0 = +1 \quad ; f_0 = 0 \\ 2F^{(+)} &= F^V \quad ; s_+ = +1 \quad ; f_+ = 0 \\ 2F^{(-)} &= F^V \quad ; s_- = -1 \quad ; f_- = 1 \end{aligned} \tag{28.11}$$

If one assumes that $F_\pi(k^2) \approx F_1^V(k^2)$ in the region of interest, then the replacement $\varepsilon_\lambda \to k_\lambda$ gives zero; hence one concludes that this current is explicitly conserved. Multipoles can be projected from this amplitude through the procedures in appendix H.

The model presented here [Wa68, Pr69, Wa72] is a simple synthesis and summary of a great deal of theoretical work on N(e, e′)Δ(1232) within a hadronic framework [Fu58, De61, Vi67, Za66, Ad68]. The result is shown as the theoretical curve in Fig. 12.9. Note that this QHD picture of the cross section to the first excited state of the nucleon holds out to $k^2 \approx 4\,\text{GeV}^2 = 100\,\text{fm}^{-2}$. The individual helicity amplitudes, which provide a much more detailed test of the picture, are compared with early experiments in [Pr70]. A coupled channel extension of this model exists that describes the inelastic form factors in the higher resonance regions in Fig. 12.8 [Pr69, Wa72].

Precise coincidence studies and measurement of all the amplitudes for all the excited states of the nucleon out to high k^2 will further challenge

https://doi.org/10.1017/9781009290616.033 Published online by Cambridge University Press

our understanding of the internal dynamics of the nucleon. Of major importance is the synthesis of a relativistic quark description of the internal dynamics of the nucleon with a meson field theory description of the dynamics of its external structure.[4] Ultimately, electron excitation of the nucleon will provide benchmark tests of *ab initio* calculations of QCD, perhaps through lattice gauge theory [Wi74].

[4] Various hybrid bag models are examined in [Bh88, Wa95].

https://doi.org/10.1017/9781009290616.033 Published online by Cambridge University Press